Dynamic analysis of a viscoelastic orthotropic cracked body using the extended finite element method

M. Toolabi[a], A. S. Fallah [a,*], P. M. Baiz [b], L.A. Louca [a]

[a] Department of Civil and Environmental Engineering, Skempton Building, South Kensington Campus, Imperial College London SW7 2AZ

[b] Department of Aeronautics, Roderic Hill Building, South Kensington Campus, Imperial College London SW7 2AZ

Abstract

The extended finite element method (XFEM) is found promising in approximating solutions to locally non-smooth features such as jumps, kinks, high gradients, inclusions, voids, shocks, boundary layers or cracks in solid or fluid mechanics problems. The XFEM uses the properties of the partition of unity finite element method (PUFEM) to represent the discontinuities without the corresponding finite element mesh requirements. In the present study numerical simulations of a dynamically loaded orthotropic viscoelastic cracked body are performed using XFEM and the *J*-integral and stress intensity factors (SIF's) are calculated. This is achieved by fully (reproducing elements) or partially (blending elements) enriching the elements in the vicinity of the crack tip or body. The enrichment type is restricted to extrinsic mesh-based topological local enrichment in the current work. Thus two types of enrichment functions are adopted viz. the Heaviside step function replicating a jump across the crack and the asymptotic crack tip function particular to the element containing the crack tip or its immediately adjacent ones. A constitutive model for strain-rate dependent moduli and Poisson ratios (viscoelasticity) is formulated. A symmetric double cantilever beam (DCB) of a generic orthotropic material (mixed mode fracture) is studied using the developed XFEM code. The same problem is studied using the viscoelastic constitutive material model implemented in ABAQUS through an implicit user defined material subroutine (UMAT). The results from XFEM correlate well with those of the finite element method (FEM). Three cases viz. static, dynamic and viscoelastic dynamic are studied. It is shown that there is an increase in the value of maximum *J*-integral when the material exhibits strain rate sensitivity.

Keywords: Extended finite element method (XFEM); Enrichment; Viscoelastic; Stress intensity factor (SIF); *J*-integral; Discontinuity

* To whom correspondence should be addressed
Tel: +44 (0)2075946028
Email: as3@imperial.ac.uk (Arash S. Fallah)

1. Introduction

The recent increase in blast and ballistic threats has led to an emerging interest by defence and civil industries in materials with high stiffness-to-weight and strength-to-weight ratios such as laminated fibre reinforced composites. In a high intensity dynamic loading scenario such as blast, composites exhibit strain-rate-dependent (viscoelastic or viscoplastic) behaviour as well as experiencing plasticity, damage and fracture. Gaining an understanding of the dynamic response of composite components or structures is inevitably contingent upon developing and utilising methods through which these phenomena can be studied most accurately. This means the method should be able to incorporate all material strain-rate-dependent characteristics as well as the associated nonlinear phenomena such as damage or fracture. Fracture is, in particular, an issue since energy absorption in a blast loaded cracked system is the determining factor in blast resistant design of such systems. A crack propagates when the rate of decrease in strain energy with increased crack length is balanced by the concomitant increase in energy due to the formation of new crack surface(s) [1]. In other words, when the G-value [2], or equivalently the K-value (stress intensity factor) [3] in linear elastic fracture mechanics, in the system exceeds a critical threshold the crack propagates. One method, capable of going beyond the traditional finite element method in dealing with fracture and nonlinear material behaviour, is the extended finite elements method (XFEM).

The extended finite element method XFEM falls within the framework of the partition of unity method (PUM), first introduced by Babuska [4], to represent discontinuities in a discretised continuum. By applying this method one can include a priori knowledge regarding the local behaviour of the solution in the finite element space. There are several possibilities conceivable with regard to alterations (enrichment) to the displacement field which result in a mesh-independent non-smooth solution [5]. Each case renders the formulation suitable for a particular type of behaviour dealing with e.g. high gradients or discontinuities, and is an improvement upon conventional FEM in many ways.

In a conventional finite element mesh, crack faces and element edges must correspond to each other, a higher resolution of mesh near the crack tip is required and re-meshing is necessary if crack propagation (discontinuity evolution) is relevant. XFEM resolves these issues by enriching the displacement function near the crack tip and faces. It eliminates the requirement of re-meshing for evolving cracks and allows the entire domain to be modelled by an initial discretisation. The application of PUM to XFEM was first discussed by Belytchko and Black [6] and improved upon by Moës et al [7]. Further developments are due to Sukumar et al. [8], Areias and Belytchko [9] who proposed the extension of the formulation to 3-D problems, Sukumar and Prévost [10] who discussed the implementation and computational aspects of the method and by Gregorie et al. [11], Belytchko et al. [12, 13] and Prabel [14] who studied dynamic crack propagation in isotropic materials.

XFEM has also been successfully applied to the study of fracture in static and dynamic problems of orthotropic media. Asadpoure and Mohammadi [15], proposed novel enrichment functions for orthotropic materials which render reformulation of interaction integral (*M*-integral) possible thus allow for obtaining modal stress intensity factors accurately. Motamedi and Mohammadi [16, 17] later used the method to study dynamic response of stationary and propagating cracks in composites. They adopted a simple crack propagation criterion based

on dynamic stress intensity factors and energy release rate to study evolution of crack in an orthotropic composite [17]. Due to the high rate of loading in a dynamic pulse loading scenario and crack tip stress and strain field singularities high strain rates in the vicinity of the tip are anticipated. Strain rate field is heterogeneous and can potentially introduce alterations to material properties in all directions.

In the present study high intensity dynamic loading of a 2-D viscoelastic orthotropic medium (replicating a generic composite) is considered. While in 2-D isotropic modelling the works of Belytscho and Black [6], Dolbow et al. [18-20], Dolbow and Nadeau [20], Daux et al. [21]and in 3-D the work of Sukumar et al. [22] can be mentioned, there are no works of literature addressing orthotropic strain-rate sensitive fracture behaviour. The viscoelastic orthotropic medium is simulated using 9 material constants that completely describe its constitutive behaviour. The constants are strain-rate sensitive which means the material depicts viscoelastic behaviour. Due to the nature of loading, fracture is expected and is the only type of discontinuity addressed. An efficient method of including enrichment functions in XFEM is by adding to the displacement field certain terms which capture jumps across the broken elements (Heaviside step function) as well as singularity near the crack tip (asymptotic crack tip functions). These are well-established in the literature. Thus extrinsic local topological enrichment is used with mesh-based features which add to the number of unknowns.

As for material behaviour only linear viscoelasticity is considered i.e. material constants are assumed linear functions of strain rates. Because of the orthotropic viscoelastic behaviour of the material under plane strain[†] conditions, the asymptotic crack tip functions will be those of orthotropic materials. Sih et al. [23], Bogy [24], Bowie and Freese [25], Barnett and Asaro [26] and Kuo and Bogy [27] have all presented works deriving the analytical stress and displacement fields around a linear crack tip in an orthotropic medium. Another work on formulation of 2-D propagating cracks has been carried out by Moës et al. [7].

In section 2 the strong and weak forms of the equilibrium equations for the problem have been illustrated. In section 3 the relevant asymptotic crack tip fields based on the work of Nobile and Carloni [28] have been presented. The general form of strain rate dependence (viscoelasticity) has been demonstrated in section 4. The XFEM formulation and the enrichment functions are illustrated in section 5. The Newmark-β method has been employed as the direct time integration method to solve the time dependent dynamic equilibrium equation and the procedure has been described in more details in section 6. Subsequently in section 7 the dynamic *J*-integral has been evaluated by using the proposed formulation of Kim and Paulino [29]. Eventually in sections 8 and 9 numerical studies have been carried out and the robustness of the method has been discussed.

2. Governing equations

2.1. Strong form

Figure.1 illustrates the domain of interest depicted by Ω bounded by boundary Γ which is partitioned in a special manner i.e.:

[†]The plane stress case is very similar and is not considered in the present work due to brevity.

$$\Gamma = \Gamma_u \cup \Gamma_t \cup \Gamma_c \;\; and \;\; \Gamma_u \cap \Gamma_t \cap \Gamma_c = \emptyset$$

The part of the boundary where essential boundary conditions act is defined as Γ_u, the traction forces $\bar{t}$ acts on boundary Γ_t so this part of the boundary is subject to natural boundary conditions and crack faces which signify a line in 2-D problems and a surface in 3-D problems, is shown by boundary Γ_c.

One of the assumptions used is that the crack faces are traction free. Hence the dynamic equilibrium equations (using continuum mechanics) can be summarised as follows:

$$\boldsymbol{\nabla}.\boldsymbol{\sigma} + \boldsymbol{b} = \rho\ddot{\boldsymbol{u}} \quad in\ \Omega \tag{1}$$
$$\boldsymbol{\sigma}.\boldsymbol{n} = \bar{\boldsymbol{t}} \quad on\ \Gamma_t \tag{2}$$
$$\boldsymbol{\sigma}.\boldsymbol{n} = \boldsymbol{0} \quad on\ \Gamma_{C^+} \tag{3}$$
$$\boldsymbol{\sigma}.\boldsymbol{n} = \boldsymbol{0} \quad on\ \Gamma_{C^-} \tag{4}$$

In the above equations (which are also referred to as the strong form of the equilibrium equations), $\boldsymbol{\sigma}$ is the Cauchy stress tensor, $\boldsymbol{n}$ the unit outward normal to specified boundary, $\boldsymbol{b}$ the body force per unit volume, ρ the material density and $\ddot{\boldsymbol{u}}(\boldsymbol{x}, t)$ the acceleration vector field.

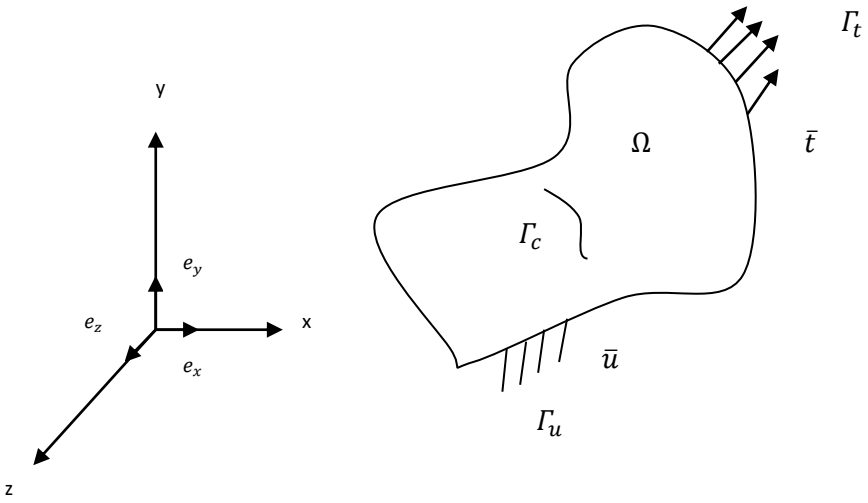


Figure 1. Initial configuration of a cracked continuum with different boundary conditions

If infinitesimal strains and small displacements are assumed the kinematic equations will be:

$$\boldsymbol{\varepsilon} = \boldsymbol{\varepsilon}(\boldsymbol{u}) = \boldsymbol{\nabla_s u} \tag{5}$$

where $\boldsymbol{u}$ is the displacement field and $\boldsymbol{\nabla_s}$ denotes the symmetric part of the gradient operator i.e.:

$$\varepsilon_{ij}\boldsymbol{e_i}\otimes\boldsymbol{e_j} = \boldsymbol{\nabla_s u} = \frac{1}{2}(u_{i,j} + u_{i,j})\boldsymbol{e_i}\otimes\boldsymbol{e_j} \tag{6}$$

and the imposed essential (displacement) boundary conditions are:

$$\boldsymbol{u} = \bar{\boldsymbol{u}}(\boldsymbol{x}, t) \qquad \text{on } \Gamma_u \tag{7}$$

Using Hooke's law the constitutive relation is as follows:

$$\boldsymbol{\sigma} = \boldsymbol{C} : \boldsymbol{\varepsilon} \tag{8}$$

where $\boldsymbol{C}$ is the constitutive tensor (In elastic problems is the material constants).

2.2 Weak form

In order to derive the weak form (or variational formulation) of the problem, it is essential to consider a space of admissible displacement fields that is defined by the totality of vector fields satisfying the essential boundary conditions and are discontinuous across the crack i.e.:

$$\boldsymbol{U} = \{\boldsymbol{v} \in \mathrm{V} \mid \boldsymbol{v} = \bar{\boldsymbol{u}} \text{ on } \Gamma_u \quad , \boldsymbol{v} \textit{ discontinuous on } \Gamma_c\} \tag{9}$$

Where, V is related to the regularity of the solution. In equation (9) discontinuous functions are allowed across the crack line. A test function space can be introduced, which is simply a perturbation to the admissible displacement field, and is thus defined as:

$$\boldsymbol{U_0} = \{\boldsymbol{v} \in \mathrm{V} \mid \boldsymbol{v} = \boldsymbol{0} \text{ on } \Gamma_u \quad , \boldsymbol{v} \textit{ discontinuous on } \Gamma_c\} \tag{10}$$

Using the principle of virtual work, the weak form of the equilibrium equations is given by:

$$\int_\Omega \rho \ddot{\boldsymbol{u}} . \boldsymbol{v} \, d\Omega + \int_\Omega \boldsymbol{\sigma} : \boldsymbol{\varepsilon}(\boldsymbol{v}) d\Omega = \int_\Omega \boldsymbol{b} . \boldsymbol{v} \, d\Omega + \int_\Gamma \bar{\boldsymbol{t}} . \boldsymbol{v} \, d\Gamma \quad \forall \, \mathbf{v} \in \boldsymbol{U_0} \tag{11}$$

Using (10), knowing $\boldsymbol{v} = \boldsymbol{0}$ on Γ_u and that crack faces are traction free ($\bar{\boldsymbol{t}} = \boldsymbol{0}$ *on* Γ_C), equation (11) simplifies to:

$$\int_\Omega \rho \ddot{\boldsymbol{u}} . \boldsymbol{v} \, d\Omega + \int_\Omega \boldsymbol{\sigma} : \boldsymbol{\varepsilon}(\boldsymbol{v}) d\Omega = \int_\Omega \boldsymbol{b} . \boldsymbol{v} \, d\Omega + \int_{\Gamma_t} \bar{\boldsymbol{t}} . \boldsymbol{v} \, d\Gamma \; \forall \, \mathbf{v} \in \boldsymbol{U_0} \tag{12}$$

Considering equations (5) and (8), equation (12) becomes:

$$\int_\Omega \rho \ddot{\boldsymbol{u}} . \boldsymbol{v} \, d\Omega + \int_\Omega \boldsymbol{\varepsilon}(\boldsymbol{u}) : \boldsymbol{C} : \boldsymbol{\varepsilon}(\boldsymbol{v}) d\Omega = \int_\Omega \boldsymbol{b} . \boldsymbol{v} \, d\Omega + \int_{\Gamma_t} \bar{\boldsymbol{t}} . \boldsymbol{v} \, d\Gamma \quad \forall \, \mathbf{v} \in \boldsymbol{U_0} \tag{13}$$

The problem would now be to find a $\boldsymbol{u} \in \boldsymbol{U}$ using equation (13). Using Green's theorem and subsequent to some manipulation it can be shown that equation (13) which is the weak form will lead to strong form equations (1)-(4). This is shown by researchers e.g. Belytschko and Black [6]. The weak form has been used in combination with XFEM for implementing and analysing the problems in this realm.

3. Crack tip displacement field

The asymptotic crack tip functions in XFEM enclose the prior knowledge of the displacement field near crack tip from classical linear elastic fracture mechanics (LEFM). Equations below are the analytical displacement fields for orthotropic material around crack tip and the corresponding constants when subjected to a uniform biaxial load as shown in Figure 2. These equations were derived by Nobile and Carloni [28]and Carloni et al. [30, 31].

$$u = \frac{2\beta}{C_{66}(p_1 - p_2)}\sqrt{2lr} \times \left\{T_2\left[\frac{p_2\sqrt{g_2(\theta)}}{l_2(\alpha - p_2^2)}cos\left(\frac{\theta_2}{2}\right) - \frac{p_1\sqrt{g_1(\theta)}}{l_1(\alpha - p_1^2)}cos\left(\frac{\theta_1}{2}\right)\right]\right.$$

$$\left. + p_1p_2T_3\left[\frac{\sqrt{g_2(\theta)}}{l_2(\alpha - p_2^2)}sin\left(\frac{\theta_2}{2}\right) - \frac{\sqrt{g_1(\theta)}}{l_1(\alpha - p_1^2)}sin\left(\frac{\theta_1}{2}\right)\right]\right\}$$

$$- \frac{2\beta p_1p_2(T_2 - p_1p_2T_1)}{C_{66}l_1l_2(\alpha - p_1^2)(\alpha - p_2^2)}(1 + rcos\theta)$$

$$- \frac{\beta T_3(p_1 + p_2)^2}{C_{66}l_1l_2(\alpha - p_1^2)(\alpha - p_2^2)}rsin\theta \qquad (14)$$

$$v = \frac{1}{C_{66}(p_1 - p_2)}\frac{\sqrt{2lr}}{l_1l_2} \times \left\{T_2\left[l_1\sqrt{g_2(\theta)}\,sin\left(\frac{\theta_2}{2}\right) - l_2\sqrt{g_1(\theta)}\,sin\left(\frac{\theta_1}{2}\right)\right]\right.$$

$$\left. + T_3\left[l_2p_2\sqrt{g_1(\theta)}\,cos\left(\frac{\theta_1}{2}\right) - l_1p_1\sqrt{g_2(\theta)}\,cos\left(\frac{\theta_1}{2}\right)\right]\right\}$$

$$+ \frac{T_3(p_1 + p_2)(l_1 - l_2)}{2C_{66}l_1l_2(p_1 - p_2)}(1 + rcos\theta)$$

$$+ \frac{(T_2 - p_1p_2T_1)}{C_{66}(p_1^2 - p_2^2)}\left(\frac{p_2}{l_1p_1} - \frac{p_1}{l_2p_2}\right)\frac{\beta T_3(p_1 + p_2)^2}{C_{66}l_1l_2(\alpha - p_1^2)(\alpha - p_2^2)}rsin\theta \qquad (15)$$

Where the material properties l_1, l_2, α and β are not of interest in this paper but can be found from Carloni et al. [31].

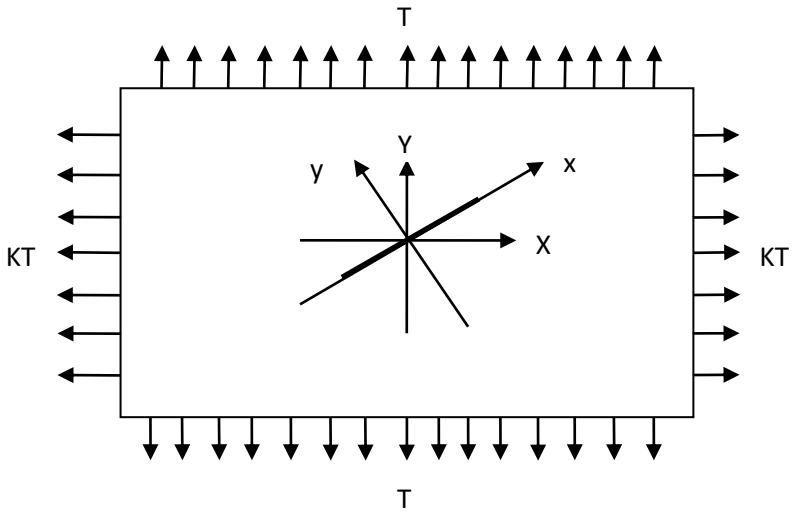


Figure 2. A cracked orthotropic body subjected to a uniform biaxial load aligned with the global coordinate system (X and Y)

The coefficients in equations (14) and (15) can be expressed as:

$$\boldsymbol{p_1 = \left(A - \left(A^2 - \frac{C_{22}}{C_{11}} \right)^{\frac{1}{2}} \right)^{\frac{1}{2}}} \quad (\mathbf{16})$$

$$\boldsymbol{p_2 = \left(A + \left(A^2 - \frac{C_{22}}{C_{11}} \right)^{\frac{1}{2}} \right)^{\frac{1}{2}}} \quad (\mathbf{17})$$

$$\boldsymbol{A = \frac{1}{2}\left[\frac{C_{66}}{C_{11}} + \frac{C_{22}}{C_{66}} - \frac{(C_{12} + C_{66})^2}{C_{11} C_{66}} \right]} \quad (\mathbf{18})$$

$$\boldsymbol{g_j(\theta) = \left(cos^2\theta + \frac{sin^2\theta}{p_j^2} \right)^{\frac{1}{2}}} \quad (\mathbf{19})$$

$$\boldsymbol{\theta_j = tan^{-1}\left(\frac{y}{p_j x} \right) = tan^{-1}\left(\frac{tan\theta}{p_j} \right)} \quad (\mathbf{20})$$

where x and y in equation (20) are the Cartesian coordinate and r and $\boldsymbol{\theta}$ are the polar coordinates, all in the local coordinate system.

4. Constitutive formulation of orthotropic viscoelasticity

The general form of the viscoelastic behaviour of the material is considered to be:

$$\boldsymbol{E_i = E_i(\dot{\varepsilon}) = E_i(\dot{\varepsilon}_{kl}),} \quad \boldsymbol{\nu_{ij} = \nu_{ij}(\dot{\varepsilon}) = \nu_{ij}(\dot{\varepsilon}_{kl}),} \quad \boldsymbol{G_{ij} = G_{ij}(\dot{\varepsilon}) = G_{ij}(\dot{\varepsilon}_{kl})} \qquad (\mathbf{21})$$

Where *i,j=1,2* due to the fact that a 2-D problem is under consideration. In this paper the only type of material strain rate dependence considered is viscoelasticity i.e. dependence of elastic constants on strain rate. Further simplification of the model is as follows:

$$\boldsymbol{E_1 = E_1(\dot{\varepsilon}_{11}) = E_{1_0} + A\dot{\varepsilon}_{11}} \qquad (\mathbf{22})$$

$$\boldsymbol{E_2 = E_2(\dot{\varepsilon}_{22}) = E_{2_0} + B\dot{\varepsilon}_{22}} \qquad (\mathbf{23})$$

$$\boldsymbol{\nu_{12} = \nu_{12}(\dot{\varepsilon}_{11}) = \nu_{12_0} + C\dot{\varepsilon}_{11}} \qquad (\mathbf{24})$$

$$\boldsymbol{G_{12} = G_{12}(\dot{\varepsilon}_{12}) = G_{12_0} + D\dot{\varepsilon}_{12}} \qquad (\mathbf{25})$$

$$\boldsymbol{\dot{\varepsilon}} = \begin{Bmatrix} \dot{\varepsilon}_{11} \\ \dot{\varepsilon}_{22} \\ \dot{\varepsilon}_{12} \end{Bmatrix} \qquad (\mathbf{26})$$

This means linear dependence of material constants upon strain rate is assumed (the first and second terms in the Mc Lauren expansion of the function) and each modulus is affected merely by the rate of straining in that direction. As for Poisson ratios the choice of the form of functional dependence concurs with Green energy imposed symmetry on the compliance matrix i.e. $\boldsymbol{E_i\nu_{ji} = E_j\nu_{ij}}$ must always be satisfied.

A, *B*, *C* and *D* are constant depending on the specific type of material behaviour. $\boldsymbol{E_{1_0}}$, $\boldsymbol{E_{2_0}}$ $\boldsymbol{\nu_{12_0}}$ and $\boldsymbol{G_{12_0}}$ are the static Young moduli in directions 1 and 2, Poisson ratio and Shear modulus of the orthotropic material. The constitutive matrix must thus be updated in each increment and depending on whether the integration procedure is implicit or explicit there may be need for iteration per increment (implicit) or a critical time increment ought to be introduced (explicit) which renders the procedure conditionally stable and computationally less expensive. The extended finite element code is implicit and the implementation of mechanical constitutive behaviour in ABAQUS is done through a user defined material subroutine (UMAT) in the implicit FE module. The study is hence restricted to implicit FE. The entries of material Jacobian matrix $\boldsymbol{J}$ are defined as ($\boldsymbol{J_{ijkl} = \frac{\partial \Delta\sigma_{ij}}{\partial \Delta\varepsilon_{kl}}}$) and updated stresses are derived as follows:

$$\boldsymbol{\sigma_{ij} = \sigma_{ij}(\varepsilon_{mn}, \dot{\varepsilon}_{mn}) = C_{ijkl}(\dot{\varepsilon}_{mn})\varepsilon_{kl}} \qquad (27)$$

$$\boldsymbol{d\sigma_{ij} = \frac{\partial \sigma_{ij}}{\partial \varepsilon_{kl}} d\varepsilon_{kl} + \frac{\partial \sigma_{ij}}{\partial \dot{\varepsilon}_{kl}} d\dot{\varepsilon}_{kl} = C_{ijkl}(\dot{\varepsilon}_{mn}) d\varepsilon_{kl} + \frac{\partial \sigma_{ij}}{\partial \dot{\varepsilon}_{kl}} d\dot{\varepsilon}_{kl}} \qquad (28)$$

Or in the more familiar incremental form as:

$$\Delta\boldsymbol{\sigma_{ij}} = \boldsymbol{C_{ijkl}}(\dot{\boldsymbol{\varepsilon}}_{\boldsymbol{mn}})\Delta\boldsymbol{\varepsilon_{kl}} + \frac{\boldsymbol{\partial\sigma_{ij}}}{\boldsymbol{\partial\dot{\varepsilon}_{kl}}}\Delta\dot{\boldsymbol{\varepsilon}}_{\boldsymbol{kl}} \tag{29}$$

5. XFEM discretisation

The XFEM introduces new functions referred to as "enrichment functions" which are added to the displacement approximation equation by considering the properties of the partition of unity method [4]. The enrichment functions are achieved either by:

1. Adding special shape functions (these functions are tailored so that they can capture jumps across cracks, singularities, etc) to the polynomial approximation space. These tailored shape functions lead to 'extrinsic enrichment'. As the result of this type of enrichment there will be more shape functions and unknowns in the approximation.

2. Replacing some or all of the shape functions in the polynomial approximation space by some special shape functions which again as in the previous method can capture singularities, jumps, etc (i.e. non-smooth solutions). As the result of this, the number of shape functions in total remains unchanged and the number of unknowns remains unaffected. This method of enrichment is referred to as 'intrinsic enrichment'.

In this paper the first method i.e. extrinsic enrichment, has been adopted. Two standard types of extrinsic, local enrichment functions are used in this work viz. the Heaviside step function and the asymptotic crack tip functions. As a result of using these enrichment functions, new degrees of freedom are introduced to calibrate the displacement field and also to interpolate values within an element. The Heaviside step function, $H(\boldsymbol{x})$, is also referred to as a discontinuous, jump or step function. It is defined in the local crack co-ordinate system as:

$$\boldsymbol{H(x)} = \begin{cases} \boldsymbol{+1} & \boldsymbol{x\ above\ the\ crack} \\ \boldsymbol{-1} & \boldsymbol{x\ below\ the\ crack} \end{cases} \tag{30}$$

The asymptotic crack tip functions (F_l for $l=1..4$) make it possible to capture the singularity of strain around crack tip within the element containing it. The functions must be tailored so that the displacement field contains all information for the orthotropic material i.e. they are of the form derived by equations (14) and (15), thus:

$$\boldsymbol{F_l} \equiv \left\{\sqrt{r}\,cos\left(\frac{\theta_1}{2}\right)\sqrt{g_1(\theta)}, \sqrt{r}\,cos\left(\frac{\theta_2}{2}\right)\sqrt{g_2(\theta)}, \sqrt{r}\,sin\left(\frac{\theta_1}{2}\right)\sqrt{g_1(\theta)}, \sqrt{r}\,sin\left(\frac{\theta_2}{2}\right)\sqrt{g_2(\theta)}\ \right\} \tag{31}$$

The third and fourth elements of the set in equation (31) capture the discontinuity across the crack where as the first two are continuous. These can be weighted and added together for enriching the nodes of elements that are either cut by the crack or contain the crack tip. This is shown in Figure.3. The approximation of displacement field using the enrichment step and crack tip functions is therefore as follows:

$$\boldsymbol{u}^h = \sum_{i \in I} \phi_i \boldsymbol{u}_i \; + \sum_{j \in J} b_j \boldsymbol{\phi}_j \, H(\boldsymbol{x}) + \sum_{k \in K^m} \boldsymbol{\phi}_k \left(\sum_{l=1}^{4} c_k^{lm} F_l^m(x) \right) \tag{32}$$

Where *I* is the set of all nodes present in the mesh, *J* represents the set of nodes whose edge is cut into two by the crack while the element does not contain the crack tip (encircled nodes in Figure 3) and K^m denotes the set of nodes in the m^{th} element that contain the crack tip (square nodes in Figure 3.).

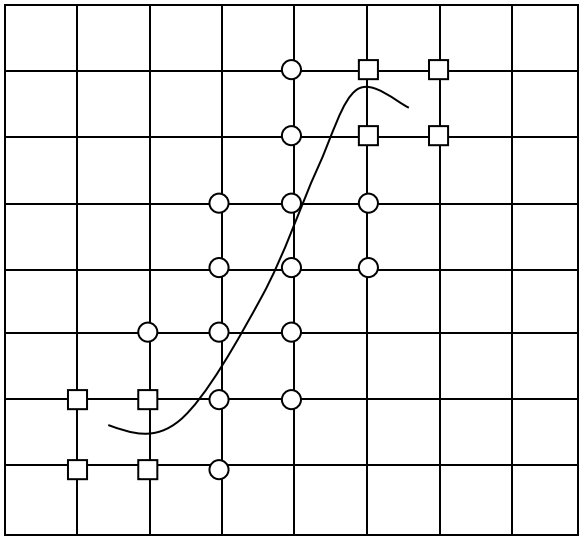


Figure 3. The XFEM mesh in the presence of a crack (Nodes enriched by crack tip functions are marked by squares and the ones enriched by Heaviside function are marked by circles)

5.1. Numerical integration of the weak form equation

Modifications have been made to element quadrature routines in order to accurately include the contribution to the weak form on both sides of the discontinuity. The reason is that cracks are allowed to be arbitrarily oriented in an element therefore the use of standard Gauss quadrature may be inaccurate. This is due to the fact that if the integration of jump functions is not realised when compared with constant functions spurious singular modes can appear in the system of equations.

The domain in which the discrete weak form is normally constructed can be expressed by:

$$\Omega = \bigcup_e \Omega_e$$

Where *e* is the index for a generic element. The elements that are cut by the crack are divided into element sub-domains whose boundaries align with the crack geometry:

$$\Omega_e = \bigcup_s \Omega_s$$

This has clearly been shown in Figure.4. In 2-D, triangular elements are usually chosen to construct sub-elements. There are different sub-elements that can be used like the ones explained in [32] by Fish who uses trapezoids instead.

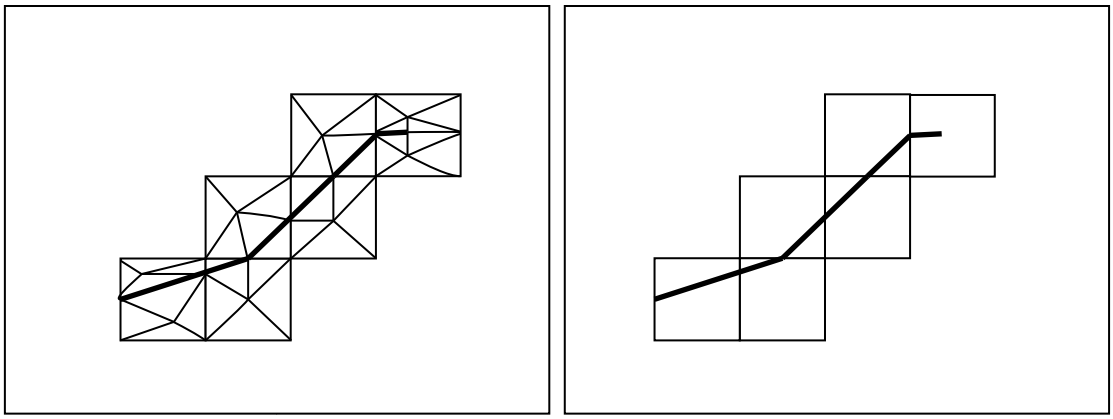


Figure 4. Triangulation procedure (On the right the crack has cut through some elements and on the left the elements that are cut by the crack are divided into triangular sub-elements in a way that their edge align with the crack interface [23])

It is important to emphasize that this method does not directly introduce extra degrees of freedom because of the new sub-elements created as a result of triangulation procedure implied; they are only constructed and used to compute the integrals involved in the weak form.

6. Solving for the dynamic response (the direct integration method)

In this paper the time integration scheme adopted to deal with the extended finite element formulation of the problem is the Newmark-β method which is an implicit method, and thus unconditionally stable. The step-by-step method below is taken from Bathe and Wilson [33] to calculate the solution after time increment *n+1*:

$$\widehat{\boldsymbol{K}}^{(n)} = \boldsymbol{K}^{(n)} + \boldsymbol{a_0}\boldsymbol{M}^{(n)} + \boldsymbol{a_1}\boldsymbol{C}^{(n)} \tag{33}$$

$$\widehat{\boldsymbol{R}}^{(n+1)} = \boldsymbol{R}^{(n+1)} + \boldsymbol{M}^{(n)}\left(\boldsymbol{a_0}\boldsymbol{U}^{(n)} + \boldsymbol{a_2}\dot{\boldsymbol{U}}^{(n)} + \boldsymbol{a_3}\ddot{\boldsymbol{U}}^{(n)}\right) + \boldsymbol{C}\left(\boldsymbol{a_1}\boldsymbol{U}^{(n)} + \boldsymbol{a_4}\dot{\boldsymbol{U}}^{(n)} + \boldsymbol{a_5}\ddot{\boldsymbol{U}}^{(n)}\right) \tag{34}$$

$$\widehat{\boldsymbol{K}}^{(n)}\boldsymbol{U}^{(n+1)} = \widehat{\boldsymbol{R}}^{(n+1)} \tag{35}$$

$$\ddot{\boldsymbol{U}}^{(n+1)} = \boldsymbol{a_0}\left(\boldsymbol{U}^{(n+1)} - \boldsymbol{U}^{(n)}\right) - \boldsymbol{a_2}\dot{\boldsymbol{U}}^{(n)} - \boldsymbol{a_3}\ddot{\boldsymbol{U}}^{(n)} \tag{36}$$

$$\dot{\boldsymbol{U}}^{(n+1)} = \dot{\boldsymbol{U}}^{(n)} + \boldsymbol{a_6}\ddot{\boldsymbol{U}}^{(n)} + \boldsymbol{a_7}\ddot{\boldsymbol{U}}^{(n+1)} \tag{37}$$

where $\boldsymbol{K}$, $\boldsymbol{M}$, and $\boldsymbol{C}$ are stiffness, mass and damping matrices. For computational efficiency $\widehat{\boldsymbol{K}}$ is triangularised, i.e. $\widehat{\boldsymbol{K}} = \boldsymbol{L}\boldsymbol{D}\boldsymbol{L}^{\boldsymbol{T}}$. $\boldsymbol{U}^{(n+1)}, \dot{\boldsymbol{U}}^{(n+1)}$ and $\ddot{\boldsymbol{U}}^{(n+1)}$ are the global nodal

displacement, nodal velocity and nodal acceleration vectors evaluated at time $\boldsymbol{t + \Delta t}$ (where $\boldsymbol{\Delta t}$ is the time increment). Constants $\boldsymbol{a_i}$ ($\boldsymbol{i = 0\ to\ 7}$) are calculated as follows:

$$\boldsymbol{a_0 = \frac{1}{\alpha \Delta t^2}} \quad (\boldsymbol{38a})$$

$$\boldsymbol{a_1 = \frac{\delta}{\alpha \Delta t}} \quad (\boldsymbol{38b})$$

$$\boldsymbol{a_2 = \frac{1}{\alpha \Delta t}} \quad (\boldsymbol{38c})$$

$$\boldsymbol{a_3 = \frac{1}{2\alpha} - 1} \quad (\boldsymbol{38d})$$

$$\boldsymbol{a_4 = \frac{\delta}{\alpha} - 1} \quad (\boldsymbol{38e})$$

$$\boldsymbol{a_5 = \frac{\Delta t}{2}\left(\frac{\delta}{\alpha} - 2\right)} \quad (\boldsymbol{38f})$$

$$\boldsymbol{a_6 = \Delta t(1 - \delta)} \quad (\boldsymbol{38g})$$

$$\boldsymbol{a_7 = \delta \Delta t} \quad (\boldsymbol{38h})$$

Where $\boldsymbol{\alpha}$ and $\boldsymbol{\delta}$ are Newmark parameters ($\boldsymbol{\delta \geq 0.5}$ and $\boldsymbol{\alpha \geq 0.25(0.5 + \delta)^2}$) which are chosen to be 0.25 and 0.5, respectively, in the present study for the unconditionally stable solution.

Due to viscoelasticity effects, the constitutive and compliance matrices will change at each time step. The crack tip enrichment functions, given by equation (31) need to be updated at each time step as $\boldsymbol{F_l = F_l(\, g_j, \theta_j)}$ (Since $\boldsymbol{g_j = g_j(P_j)}$ in equation (19), $\boldsymbol{\theta_j = \theta_j(P_j)}$ in equation (20) and $\boldsymbol{P_j = P_j(C_{ij})}$ in equations (16) and (17) where $\boldsymbol{C_{ij}}$ are the constitutive coefficients).

7. Stress intensity factors (SIF's) calculation

The path independent J-integral introduced by Rice [34]is used for calculation of energy release rate and indirectly of the stress intensity factors. The dynamic form of the J-integral is presented by Nishioka and Atluri [35] as:

$$J_k = \int_{\Gamma} \left[(W + K)n_k - \ t_i u_{j,k}\right] d\Gamma + \int_{V_\Gamma} \left(\rho \ddot{u}_i u_{i,k} - \rho \dot{u}_{i,k} \dot{u}_i\right) dA \quad (39)$$

Where Γ is the contour surrounding the crack tip, V_Γ is the area within contour Γ, W is the strain energy density i.e. $W = \frac{1}{2}\sigma_{ij}\varepsilon_{ij}$, K is kinetic energy density i.e. $K = \frac{1}{2}\rho\dot{u}_i\dot{u}_i$, n_k is the k^{th} component of the outward unit normal to Γ, $t_i = \sigma_{ij}n_j$ is the traction, ρ is the density and $u_i, \dot{u}_i, \ddot{u}_i$ are the displacement, velocity and acceleration, respectively. Using Gauss's divergence theorem and multiplying by q function introduced by Kim and Paulino [29], equation (39) can be transformed to:

$$J_k = \int_{V_\Gamma} \left[\sigma_{ij}u_{j,k} - (W + K)\right]q_{,k}\, dA + \int_{V_\Gamma} \left(\rho\ddot{u}_i u_{i,k} - \rho\dot{u}_{i,k}\dot{u}_i\right)dA \qquad k = 1, 2 \qquad (40)$$

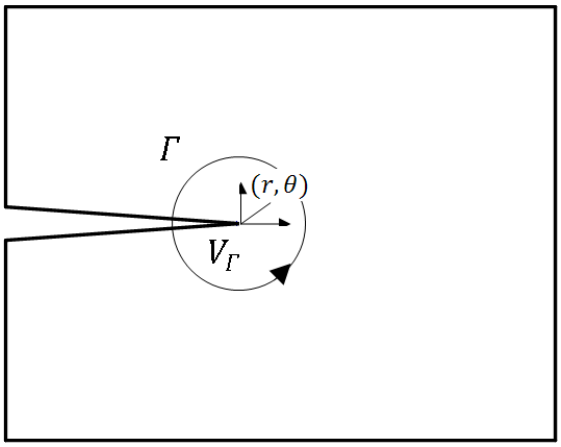


Figure 5. Contour around the crack tip and the relevant path Γ and the enclosed area V_Γ

Where k = 1 (for horizontal crack) represents the crack axis, tangential component of the dynamic J-integral. The smooth q function is assumed to vary linearly from one near the crack tip to zero at the exterior of the boundary Γ.

In non-propagating crack problems the dynamic energy release rate, G can be related to stress intensity factors by using the method introduced by Wu as given in [36] as follows:

$$G = J_1 \cos\theta_0 + J_2 \sin\theta_0 \qquad (41)$$

$$G = \frac{1}{2}\boldsymbol{K^T L^{-1} K} \qquad (42)$$

Where θ_0 is the crack angle, **K** is the stress intensity vector and the non-zero components of the **L** matrix are introduced by Dongye and Ting [37], and Ting [38]as:

$$L_{33} = \sqrt{C_{55}C_{44}} \qquad (43)$$

$$\sqrt{C_{66}C_{22}}L_{11} = \sqrt{C_{66}C_{11}}L_{22} = AB^{-\frac{1}{2}} \qquad (44)$$

$$A = (C_{11}C_{22} - C_{12}^2)C_{66} \qquad (45)$$

$$B = (C_{66} + \sqrt{C_{11}C_{22}})^2 - (C_{12} + C_{66})^2 \qquad (46)$$

Where C_{ij} are the constitutive coefficients. The mixed mode stress intensity factors can be evaluated from the dynamic J-integral using the method introduced by Aliabadi et al. [39]. It connects the crack face opening and sliding to the stress intensity factors by the displacement and stress fields around the crack tip derived by Sih et al. [23]:

$$\begin{Bmatrix} \delta_I \\ \delta_{II} \end{Bmatrix} = \sqrt{\left(\frac{8r}{\pi}\right)} \begin{bmatrix} D_{11} & D_{12} \\ D_{21} & D_{22} \end{bmatrix} \begin{Bmatrix} K_I \\ K_{II} \end{Bmatrix} \tag{47}$$

$$D_{11} = Im\left(\frac{\mu_2 p_1 - \mu_1 p_2}{\mu_1 - \mu_2}\right), D_{12} = Im\left(\frac{p_1 - p_2}{\mu_1 - \mu_2}\right), D_{21} = Im\left(\frac{\mu_2 q_1 - \mu_1 q_2}{\mu_1 - \mu_2}\right), D_{22} = Im\left(\frac{q_1 - q_2}{\mu_1 - \mu_2}\right) \tag{48}$$

Where p_i, q_i are defined as:

$$p_i = a_{11}\mu_i^2 + a_{12} - a_{16}\mu_i \tag{49}$$

$$q_i = a_{12}\mu_i + \frac{a_{22}}{\mu_i} - a_{26} \tag{50}$$

a_{ij} are the compliance coefficients and μ_i can be computed from the equation introduced by Lekhnitskii [40] for a crack in an orthotropic body with general boundary conditions and subjected to arbitrary forces:

$$a_{11}\mu^4 - 2a_{16}\mu^3 + (2a_{12} + a_{66})\mu^2 - 2a_{26}\mu + a_{22} = 0 \tag{51}$$

The roots of equation (51) are either complex or have imaginary parts only and are in conjugate pairs as it has been shown by Lekhnitskii [40] in his work. Adopting equations (47) to (51), the variables, Z (the ratio of the crack face opening to sliding displacement) and H (the dynamic stress intensity factors ratio) are introduced as:

$$Z = \frac{\delta_{II}}{\delta_I} = \frac{D_{21}K_I + D_{22}K_{II}}{D_{11}K_I + D_{12}K_{II}} \tag{52}$$

$$H = \frac{K_I}{K_{II}} = \frac{D_{21}Z - D_{22}}{D_{21} + D_{11}Z} \tag{53}$$

The stress intensity factors are then calculated using equations (52) and (53).

8. Case studies

In this paper a 2-D plane geometry with a horizontal edge crack known as a double cantilever beam (DCB), made of a generic orthotropic material with different material orientation angles has been considered. The purpose is twofold, (1) to study the effect of viscoelasticity and the difference it makes to fracture related response parameters, (2) to illustrate and discuss the accuracy of the method that has been used. Two types of material viscoelasticity examples are considered here, one is material with low dependency on viscoelasticity (which in this case the results are expected to be close to dynamic results) and one with high dependency on viscoelasticity. The results and the accuracy of the method obtained from FEM (ABAQUS-UMAT user subroutine code) and

XFEM are compared in each example. In both cases plane strain condition is assumed with dimensions of the domain being, $\boldsymbol{W = 3000\,mm}$, $\boldsymbol{L = 2h = 1500\,mm}$, $\boldsymbol{a = 1000\,mm}$ (see figure 7). Ω is the angle of orientation of the orthotropic material. The initial material properties that are considered here are: $\boldsymbol{E_{1_0} = 100\,GPa}$, $\boldsymbol{E_{2_0} = 70\,GPa}$, $\boldsymbol{G_{12_0} = 50\,GPa}$, $\boldsymbol{\nu_{12_0} = 0.2}$ and $\boldsymbol{\rho = 2000\ kg/m^3}$. A dynamic ramp tensile UDL load is applied to the top and bottom of the DCB alike with rise time to maximum depicted by $\boldsymbol{t_r}$ (figure 6). The XFEM mesh of the model in figure 7 consists of a $\boldsymbol{60 \times 10}$ square element mesh.

An FE model of the same problem was set-up, analysed, and studied using ABAQUS-standard which uses implicit FE formulation for the calculation of J-integral. A user defined material subroutine (UMAT) is developed and used to replicate the specific constitutive behaviour of the viscoelastic material under consideration. Stress intensity factors are not available as output variables when user material subroutines such as UMAT are used in conjunction with built-in capabilities. Figures 8 (a) and 8 (b) depict the FE and XFEM meshes, respectively. The FE model of a typically deformed profile of dynamically loaded DCB under study (Figure 8 (a)) has a mesh size is 62 mm with much finer mesh being used in the vicinity of the crack tip to ensure accurate realisation of singularity there. The number of nodes and elements in the model are 6791 and 2196, respectfully, which means the total number of unknown variables in the problem mounts to 13582 including any Lagrange multipliers. The XFEM mesh shows the corresponding mesh with a typical contour around the crack tip as well as Heaviside step function (circled) and asymptotic crack tip function enriched (squared) nodes. In the FE model CPE8R elements i.e. 8-node biquadratic plane strain quadrilateral, reduced integration elements were used throughout and the elements around the crack tip were collapsed to correctly simulate the square root singularity at the tip (see Figure 9).

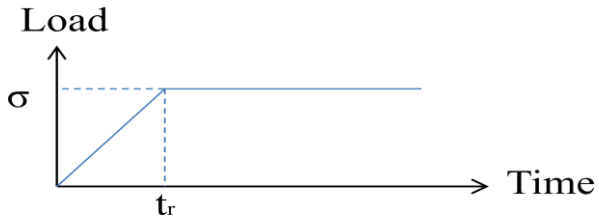


Figure 6. Dynamic tension loading with rise time $\boldsymbol{t_r}$

As for constitutive formulation in the first case in the limit constant *A* in equation (22) is considered to be zero (for small strain rate effect). The results of the computed mixed mode stress intensity factors for both FEM and XFEM are shown in figures 10-15. The results from XFEM (with coarse mesh) are in very good agreement with FEM (with fine mesh) as discussed in the sequel.

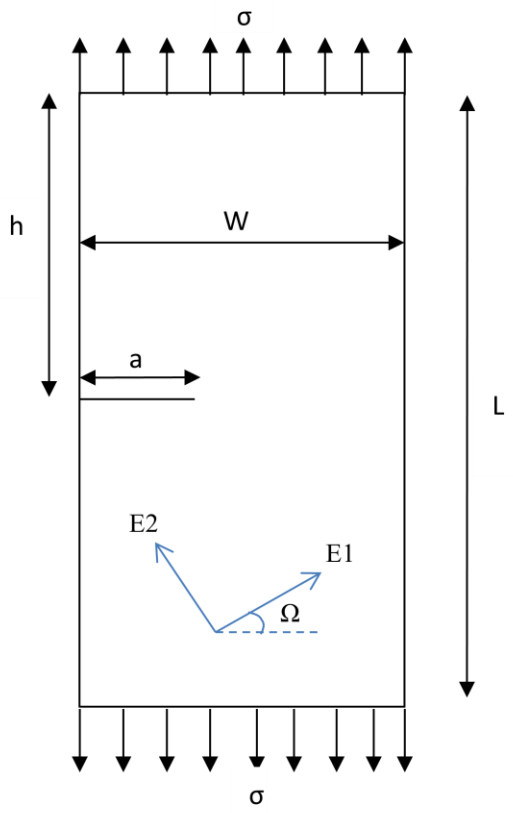
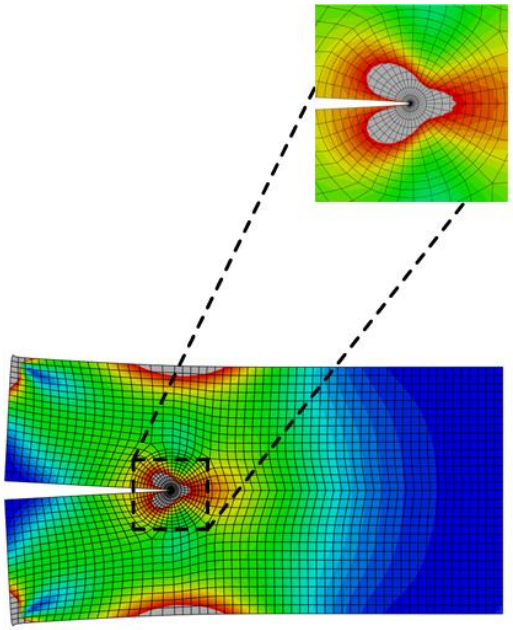
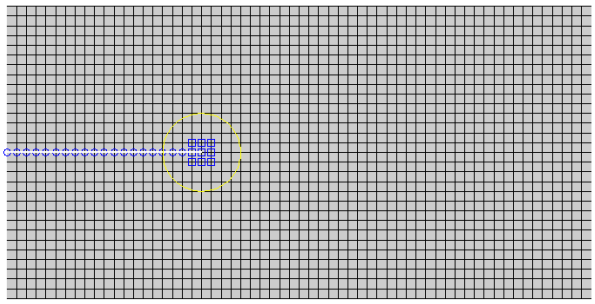


Figure 7. The rectangular 2-D geometry with plane strain formulation and a horizontal edge crack



(a)

Figure 8. (a) The finite element model of rectangular 2-D geometry with plane strain conditions and a horizontal edge crack (ABAQUS), (b) the finite element mesh for the XFEM code



(b)

Figure 8. Cont'd

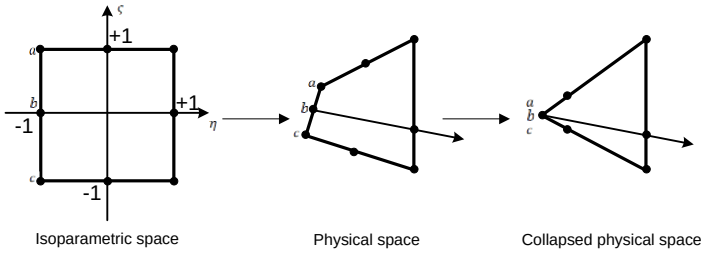


Figure 9: Collapsing procedure for quadratic elements used in simulation of singularity in ABAQUS

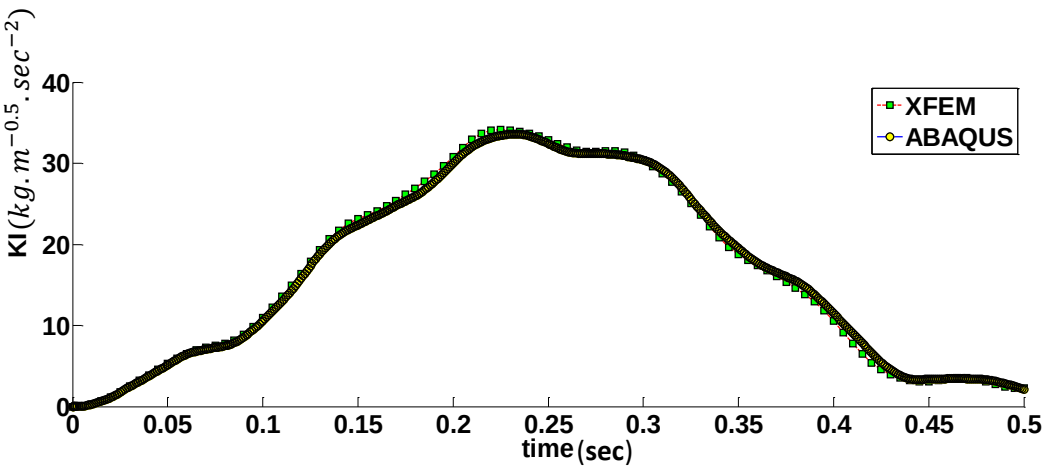


Figure 10. Dynamic mode I stress intensity factor (KI) for $\boldsymbol{t_r = 0.024}$ sec and $\boldsymbol{\Omega = 30^{\circ}}$

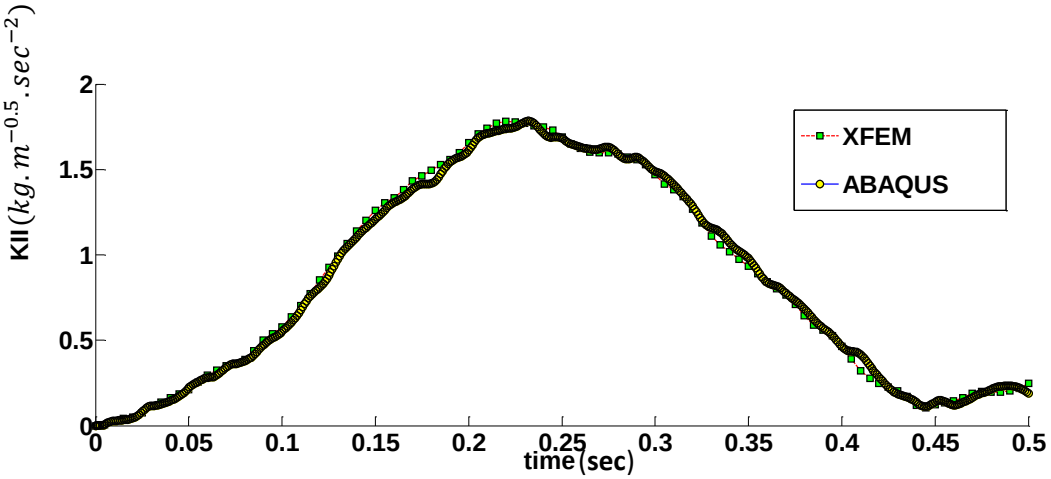


Figure 11. Dynamic mode II stress intensity factor (KII) for $\boldsymbol{t_r = 0.024}$ sec and $\boldsymbol{\Omega = 30^{\circ}}$

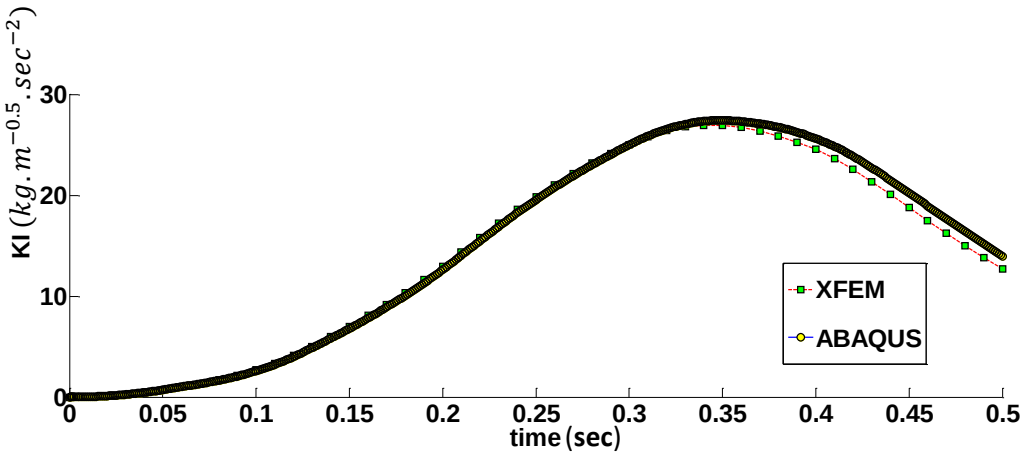


Figure 12. Dynamic mode I stress intensity factor (KI) for $\boldsymbol{t_r = 0.236}$ sec and $\boldsymbol{\Omega = 30^{\circ}}$

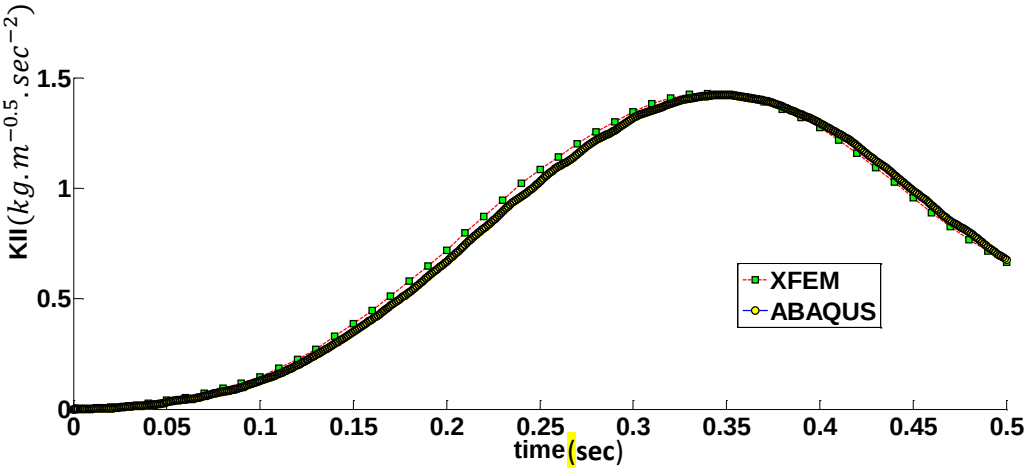


Figure 13. Dynamic mode II stress intensity factor (KII) for $\boldsymbol{t_r = 0.236}$ sec and $\boldsymbol{\Omega = 30^{\circ}}$

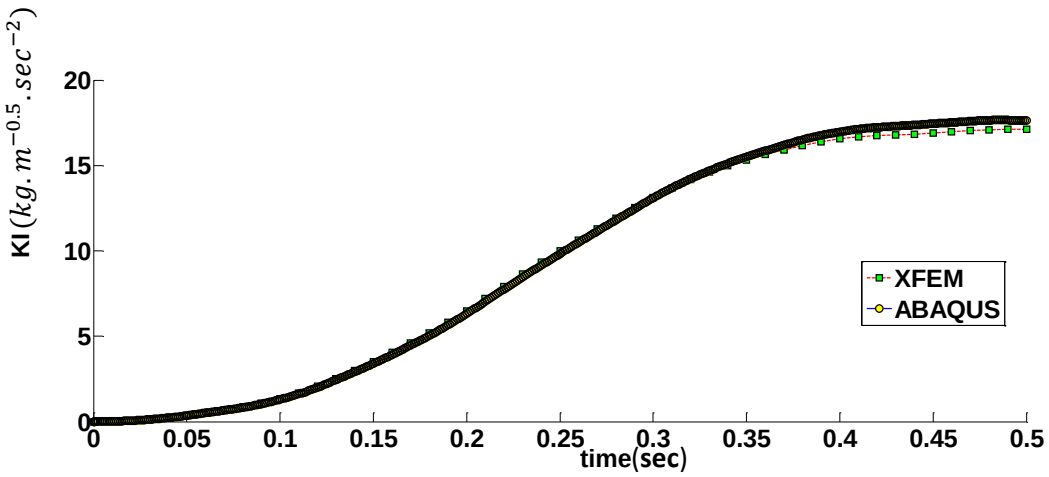


Figure 14. Dynamic mode I stress intensity factor (KI) for $\boldsymbol{t_r = 0.471}$ sec and $\boldsymbol{\Omega = 30^{\circ}}$

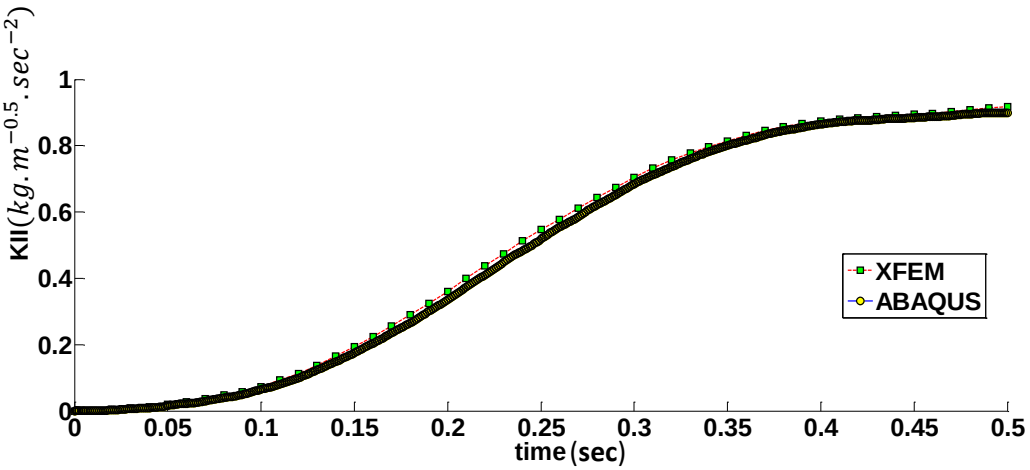


Figure 15. Dynamic mode II stress intensity factor (KII) for $\boldsymbol{t_r = 0.471}$ sec and $\boldsymbol{\Omega = 30^{\circ}}$

In the second case the constant *A* in equation (22) is chosen to be $\mathbf{10^8}$. In this example the non-dimensional J-integral (normalised with respect to the static J-integral) for both FEM and XFEM are computed instead of stress intensity factors and the results are again in good agreement (See figures 16-20).

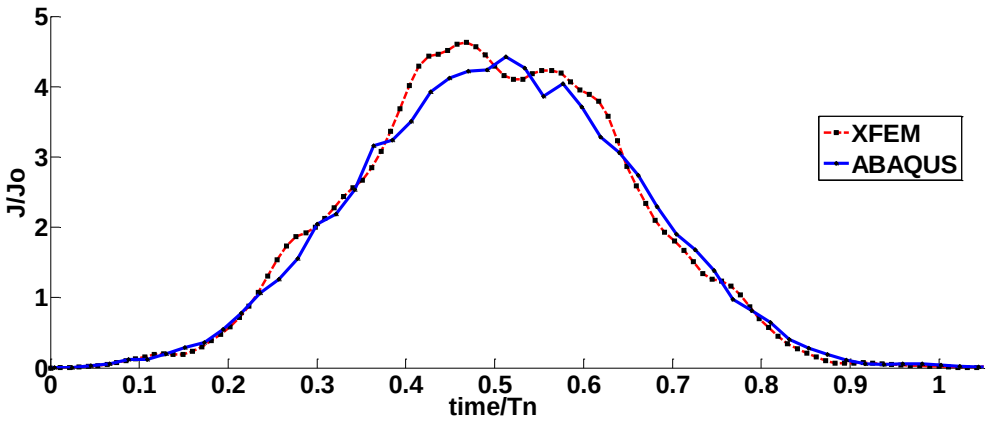


Figure 16. Vsicoelastic dynamic J-integral for $t_r = 0.0024$ sec and $\Omega = 0^{\circ}$

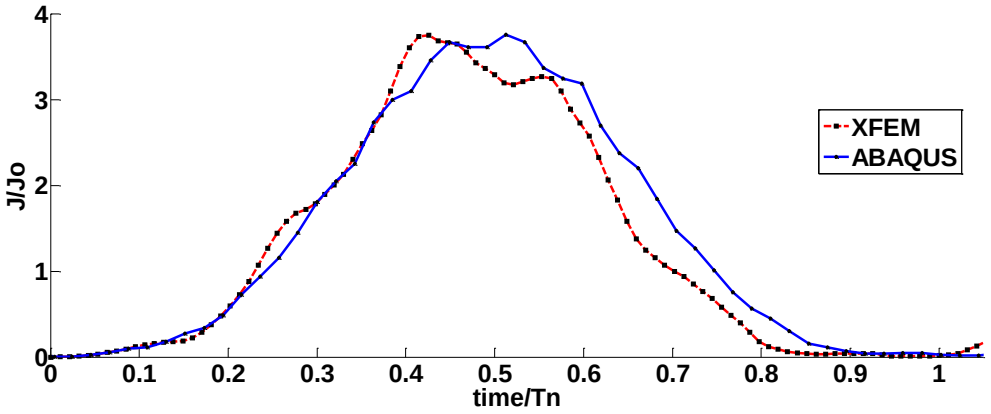


Figure 17. Viscoelastic dynamic J-integral for $t_r = 0.0024$ sec and $\Omega = 30^{\circ}$

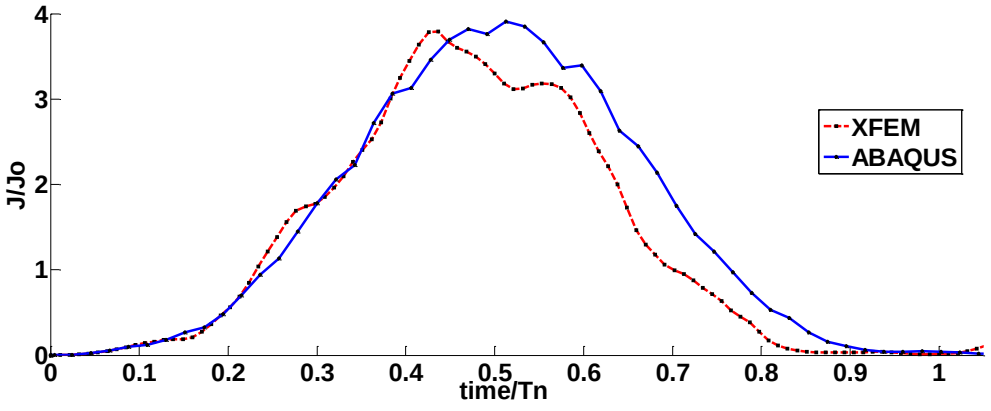


Figure 18. Viscoelastic dynamic J-integral for $t_r = 0.0024$ sec and $\Omega = 45^{\circ}$

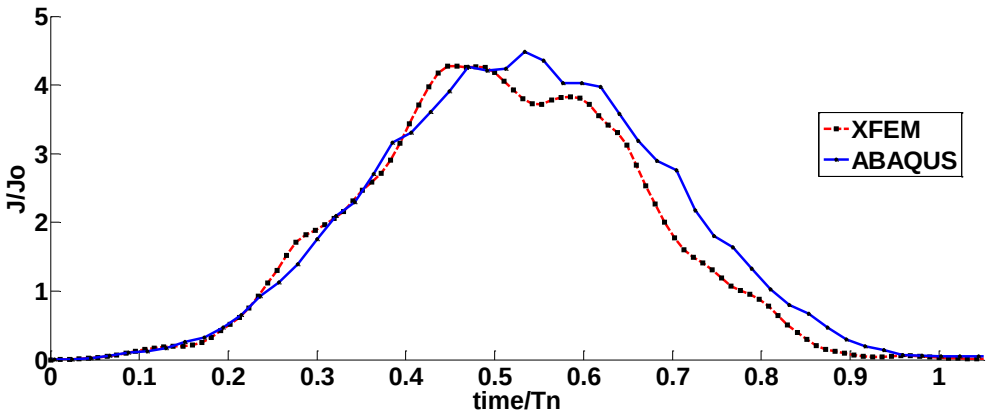


Figure 19. Viscoelastic dynamic J-integral for $\boldsymbol{t_r = 0.0024}$ sec and $\boldsymbol{\Omega = 60^{\circ}}$

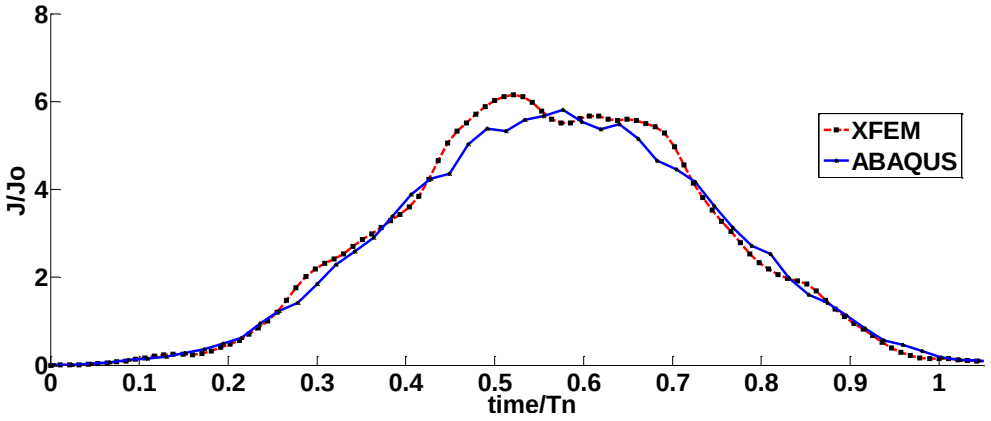


Figure 20. Vsicoelastic dynamic J-integral for $\boldsymbol{t_r = 0.0024}$ sec and $\boldsymbol{\Omega = 90^{\circ}}$

In the dynamic analysis of blast loaded cracked bodies the maximum value of the J-integral or modal stress intensity factors is of interest since this parameter defines stationary or propagating nature of the crack therefore the maximum values of J-integral for all material axes of orthotropic orientation have been compared (figures 21 and 22). The results show that the percentage of difference between the maxima J-integral values computed using the in-house developed XFEM code and conventional FEM contour integral option is bounded to 6% for different material orientation angles.

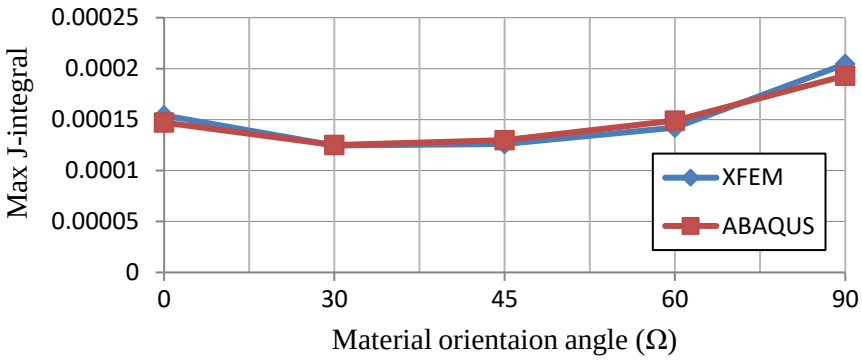


Figure 21. Maximum dynamic J-integral for different material orientation angle

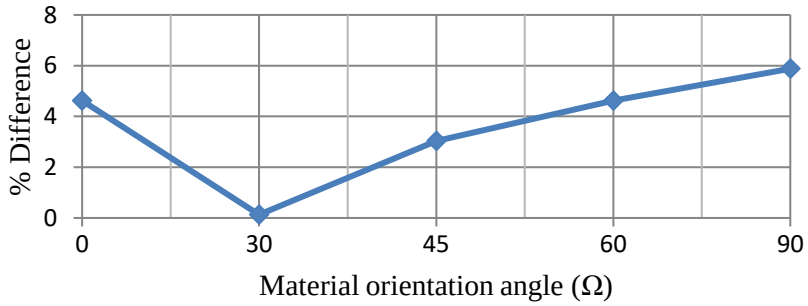


Figure 22. Percentage difference between the maximum J-integral calculated using XFEM from ABAQUS

9. Conclusion

In this paper the extended finite element method (XFEM) was used to analyse a 2-D cracked body made of a viscoelastic orthotropic material. The cracked body has a stationary edge crack and can be assumed a DCB. Only linear viscoelasticity is considered. The method was used to capture modal stress intensity factors and the J-integral for low and high viscoelasticity dependency. The dynamic mixed mode stress intensity factors and the dynamic J-integral were compared with the results obtained from ABAQUS (FEM). In order to model the constitutive linear viscoelastic behaviour a user defined material subroutine (UMAT) was developed for ABAQUS. As extreme dynamic loads as blast and impact were in mind the maxima of fracture related parameters were deemed more significant than the detailed time-history of these parameters. The difference between the maximum values of J-integral obtained from XFEM and those extracted from FEM was found to be bound to 6% when the material orientation angle was 90 degrees. This is due to the fact that more strain-rate dependence is expected in the matrix direction in a composite than in the fibre direction. The study also reconfirms the fact that in the analyses using XFEM a coarse mesh would suffice for the same domain to obtain good results when compared with the fine mesh used in standard FEM (e.g. using ABAQUS).

References:

[1] Gurtin ME. Thermodynamics and the griffith criterion for brittle fracture. International Journal of Solids and Structures. 1979;15:553-60.
[2] Griffith AA. The Phenomena of Rupture and Flow in Solids. Philosophical Transactions of the Royal Society of London Series A, Containing Papers of a Mathematical or Physical Character. 1921;221:163-98.
[3] Irwin GR. Analysis of Stresses and Strains Near the End of a Crack Traversing a Plate. J Appl Mech. 1957.
[4] Babuska I, Melenk JM. THE PARTITION OF UNITY METHOD. International Journal for Numerical Methods in Engineering. 1997;40:727-58.
[5] Belytschko T, Gracie R, Ventura G. A review of extended/generalized finite element methods for material modeling. Modelling and Simulation in Materials Science and Engineering. 2009;17:043001.
[6] Belytschko T, Black T. Elastic crack growth in finite elements with minimal remeshing. International Journal for Numerical Methods in Engineering. 1999;45:601-20.
[7] Moës N, Dolbow J, Belytschko T. A finite element method for crack growth without remeshing. International Journal for Numerical Methods in Engineering. 1999;46:131-50.
[8] Sukumar N, Moës N, Moran B, Belytschko T. Extended finite element method for three-dimensional crack modelling. International Journal for Numerical Methods in Engineering. 2000;48:1549-70.
[9] Areias PMA, Belytschko T. Analysis of three-dimensional crack initiation and propagation using the extended finite element method. International Journal for Numerical Methods in Engineering. 2005;63:760-88.
[10] Sukumar N, Prévost JH. Modeling quasi-static crack growth with the extended finite element method Part I: Computer implementation. International Journal of Solids and Structures. 2003;40:7513-37.
[11] Grégoire D, Maigre H, Réthoré J, Combescure A. Dynamic crack propagation under mixed-mode loading – Comparison between experiments and X-FEM simulations. International Journal of Solids and Structures. 2007;44:6517-34.
[12] Belytschko T, Chen H, Xu J, Zi G. Dynamic crack propagation based on loss of hyperbolicity and a new discontinuous enrichment. International Journal for Numerical Methods in Engineering. 2003;58:1873-905.
[13] Belytschko TED, Chen HAO. SINGULAR ENRICHMENT FINITE ELEMENT METHOD FOR ELASTODYNAMIC CRACK PROPAGATION. International Journal of Computational Methods. 2004;01:1-15.
[14] Prabel B, Marie S, Combescure A. Using the X-FEM method to model the dynamic propagation and arrest of cleavage cracks in ferritic steel. Engineering Fracture Mechanics. 2008;75:2984-3009.
[15] Asadpoure A, Mohammadi S. Developing new enrichment functions for crack simulation in orthotropic media by the extended finite element method. International Journal for Numerical Methods in Engineering. 2007;69:2150-72.
[16] Motamedi D, Mohammadi S. Dynamic analysis of fixed cracks in composites by the extended finite element method. Engineering Fracture Mechanics. 2010;77:3373-93.
[17] Motamedi D, Mohammadi S. Dynamic crack propagation analysis of orthotropic media by the extended finite element method. International Journal of Fracture. 2010;161:21-39.
[18] Dolbow J. A finite element method for crack growth without remeshing. International Journal for Numerical Methods in Engineering. 1999;46:131.
[19] Dolbow J. Discontinuous enrichment in finite elements with a partition of unity method. Finite Elements in Analysis and Design. 2000;36:235.
[20] Dolbow JE. On the use of effective properties for the fracture analysis of microstructured materials. Engineering Fracture Mechanics. 2002;69:1607.

[21] Daux C, Moës N, Dolbow J, Sukumar N, Belytschko T. Arbitrary branched and intersecting cracks with the extended finite element method. International Journal for Numerical Methods in Engineering. 2000;48:1741-60.
[22] Sukumar N. Extended finite element method for three‐dimensional crack modelling. International Journal for Numerical Methods in Engineering. 2000;48:1549.
[23] Sih GC, Paris PC, Irwin GR. On cracks in rectilinearly anisotropic bodies. International Journal of Fracture. 1965;1:189-203.
[24] Bogy DB. The plane solution for anisotropic elastic wedges under normal and shear loading. Journal of applied mechanics. 1972;39:1103.
[25] Bowie O, Freese C. Central crack in plane orthotropic rectangular sheet. International Journal of Fracture. 1972;8:49-57.
[26] Barnett DM, Asaro RJ. The fracture mechanics of slit-like cracks in anisotropic elastic media. Journal of the Mechanics and Physics of Solids. 1972;20:353-66.
[27] Kuo MC. Plane solutions for the displacement and traction-displacement problems for anisotropic elastic wedges. Journal of applied mechanics. 1974;41:197.
[28] Nobile L. Fracture analysis for orthotropic cracked plates. Composite Structures. 2005;68:285.
[29] Kim JH. The interaction integral for fracture of orthotropic functionally graded materials: evaluation of stress intensity factors. International Journal of Solids and Structures. 2003;40:3967.
[30] Carloni C. Crack initiation behaviour of orthotropic solids as predicted by the strain energy density theory. Theoretical and applied fracture mechanics. 2002;38:109.
[31] Carloni C. An alternative complex variable formulation for an inclined crack in an orthotropic medium. Engineering Fracture Mechanics. 2003;70:2033.
[32] Fish J. Finite element method for localization analysis 1989.
[33] Bathe KJ, Wilson EL. Stability and accuracy analysis of direct integration methods. Earthquake Engineering & Structural Dynamics. 1972;1:283-91.
[34] Rice JR. A Path Independent Integral and the Approximate Analysis of Strain Concentration by Notches and Cracks. Journal of applied mechanics. 1968;35:379.
[35] Nishioka T. Path-independent integrals, energy release rates, and general solutions of near-tip fields in mixed-mode dynamic fracture mechanics. Engineering Fracture Mechanics. 1983;18:1.
[36] Wu KC. Dynamic crack growth in anisotropic material. International Journal of Fracture. 2000;106:1.
[37] Dongye C. Explicit expressions of Barnett-Lothe tensors and theirs associated tensors for orthotropic materials. Quarterly of applied mathematics. 1989;47:723.
[38] Ting TCT. Barnett-Lothe tensors and their associated tensors for monoclinic materials with the symmetry plane at x3= 0. Journal of elasticity. 1992;27:143.
[39] Aliabadi MH. Crack growth analysis in homogeneous orthotropic laminates. Composites science and technology. 1998;58:1697.
[40] Lekhnitskii S. Theory of an anisotropic elastic body. San Francisco: Holden-Day; 1963.